Application of unimolecular reaction rate theory for highly flexible transition states to the dissociation of NCNO into NC and NO

S. J. Klippenstein, L. R. Khundkar, A. H. Zewail, and R. A. Marcus
Arthur Amos Noyes Laboratory of Chemical Physics, California Institute of Technology, Pasadena, California 91125[a)]

(Received 7 June 1988; accepted 11 July 1988)

A recently described method for implementing RRKM theory for unimolecular reactions with highly flexible transition states is applied to the calculation of energy and angular momentum resolved rate constants and rotational–vibrational energy distributions for the reaction $NCNO \xrightarrow{h\nu} NCNO^* \rightarrow NCNO(\text{vib. hot}) \rightarrow NC + NO$. The dissociation rate results are compared to the recent experimental results of Khundkar *et al.*, and the vibrational and rotational distribution results are compared to the experimental values of Nadler *et al.* Comparison is also made with phase space theory calculations. The calculated rotational distributions at energies below the vibrational threshold of the products are the same as those of PST. At energies (2348, 2875 cm^{-1}) above this threshold energy the rovibrational distribution is in better agreement with the data than is that of PST. The need for obtaining more accurate *ab initio* potential energy surfaces is noted, particularly for treating reactions at still higher energies.

I. INTRODUCTION

Recent detailed experimental results for energy-resolved reaction rates have been compared with several simplified models of the transition state. In particular, the energy and partially angular momentum resolved reaction rate constants for the unimolecular dissociation of NCNO determined by Khundkar *et al.*[1] via picosecond photofragment spectroscopy in a molecular beam could not be fit[1] using a tight transition state form of RRKM theory,[2] i.e., one having transitions state modes that are treated as harmonic oscillators. Neither could the energy dependence of the rates be fit to phase space theory (used to obtain phase space distributions) where the transition state is postulated to consist of two fragments which rotate freely and all degenerate electronic states are included. As they noted, too, there was also uncertainty[1] in comparing the results with phase space theory[3] regarding the role played by the near-degeneracy of the various electronic states at large distances where phase space theory (PST) has its "transition state."

It is desirable, therefore, to explore a more detailed model of the transition state (TS), as part of a study on the suitability of statistical models for rates and product state distributions. The rotational and vibrational energy distributions of the products of the same dissociation reaction have been experimentally determined by Nadler *et al.*[4] and were in good agreement with those predicted by PST when the energy was below that needed to produce vibrationally excited fragments. Some deviations were found at somewhat higher energies. In the case of RRKM theory some added assumption regarding the dynamics in the exit channel is needed for predicting product energy distributions. One such a dynamical approximation was described recently[5] in conjunction with a recent implementation of RRKM theory.[6–8] The results of this method will be compared with the experimentally determined vibrational–rotational distributions for NCNO, together with the results of RRKM theory for the rate constants themselves.

In the present treatment the transformation of the bending modes of the reactant to the hindered rotations of the TS and then finally to the free rotations of the products is considered, using a potential energy surface. In addition, the coupling of these hindered rotational modes with the overall rotations is included. Examples of this variational implementation of RRKM theory for flexible transition states of other systems are given in several recent papers[6–8] from this laboratory. In the nomenclature of Refs. 6–8 the modes which change their nature appreciably are termed the transitional modes and the remaining modes, excluding the reaction coordinate, the conserved modes. In this work the full coupling between the various transitional modes is considered together with conservation of total angular momentum. The method is based on Monte Carlo integration of the phase space volume for the transitional modes, convoluted with the distribution of the conserved modes, treated quantum mechanically. A given potential energy surface is used, together with an assumed separability of the conserved modes from the transitional modes. In the TS region the conserved modes are treated as quantum mechanical oscillators while the transitional modes are treated classically but otherwise generally for any given potential energy surface.

In the present article this implementation of RRKM theory is applied to the calculation of rate constants and product state distributions for the NCNO dissociation. There are four potential energy surfaces involved in the TS region, namely the two singlet states S_0 and S_1 and the two triplet states T_1 and T_2 which correlate to the $^2\Sigma CN + {}^2\Pi_{1/2}NO$ and $^2\Sigma CN + {}^2\Pi_{3/2}NO$ states. Consideration is given to which states are involved in determining the TS. At the present time, the potential energy surfaces for the TS region of unimolecular dissociations are not well known,

[a)] Contribution No. 7788.

and so the dependence of the results on various model potential energy surfaces is also discussed. The results obtained may then be used as a guide for the subsequent determination of an *ab initio* or improved semiempirical potential energy surface in the TS region. In Sec. II a brief description of the theoretical determination of the number of states for the highly flexible TS of NCNO is given. Results for the present k_{EJ} calculations are given in Sec. III, and are discussed in Sec. IV. In Sec. V the corresponding results for the NC and NO rovibrational distributions are given and discussed, and are followed by concluding remarks in Sec. VI.

II. THEORY

The specific rate constant k_{EJ} for unimolecular dissociation at a given energy E and total angular momentum quantum number J is given by[2]

$$k_{EJ} = N^{\dagger}_{EJ}/h\rho_{EJ}, \tag{1}$$

where ρ_{EJ} is the density of states for the reactant at the given E and J. The quantity $N^{\dagger}_{EJ}$ is the number of available quantum states of the TS with energy less than or equal to E and with the given J.

When a tight transition state is used in RRKM theory, harmonic frequencies are usually assumed for the various vibrational modes and some rotational constants are employed for the TS. $N^{\dagger}_{EJ}$ is then determined through a direct count of the available vibrational–rotational states at the given energy and total angular momentum.

In phase space theory[3] (PST) the TS involves two freely rotating fragments, whose vibrational modes are those of the fragments themselves. The rotational modes are approximated as free rotations. An attractive fragment–fragment potential of the form R^{-n} is used, where n is usually 6 and R is the dissociation coordinate. In the present application the dissociation coordinate R is chosen to be the separation distance between the centers of masses of the NC and NO fragments. In PST effective barriers are calculated as a function of the orbital angular momentum quantum number of the two fragments l, and $N^{\dagger}_{EJ}$ denotes the total number of these virational–rotational–orbital states which satisfy the total angular momentum conservation rule and have an energy greater than that of the l-dependent effective barrier. The allowed l's are those consistent with the triangular inequality for the total angular momentum and with a radial kinetic energy sufficient to exceed the barrier's maximum. The $R^{\dagger}$ of the latter varies with l, and so there are a number of such $R^{\dagger}(l)$'s for the given J.

In Refs. 7 and 8 it has been shown how conventional coordinates may be used in an implementation of RRKM theory developed by Wardlaw and Marcus to treat these highly flexible transition states. They used action-angle variables to facilitate the imposition of the constraint of fixed total angular momentum. In Ref. 7 a convenient way for imposing this constraint using conventional coordinates was presented. In these studies an approximate separation of variables into the conserved and transitional modes mentioned earlier is introduced. In the present article the method of Refs. 7 and 8 is used in all determinations of $N_{EJ}(R)$. In particular, a computational method based on Eqs. (12), (13), and (17)–(21) of Ref. 8 is employed.

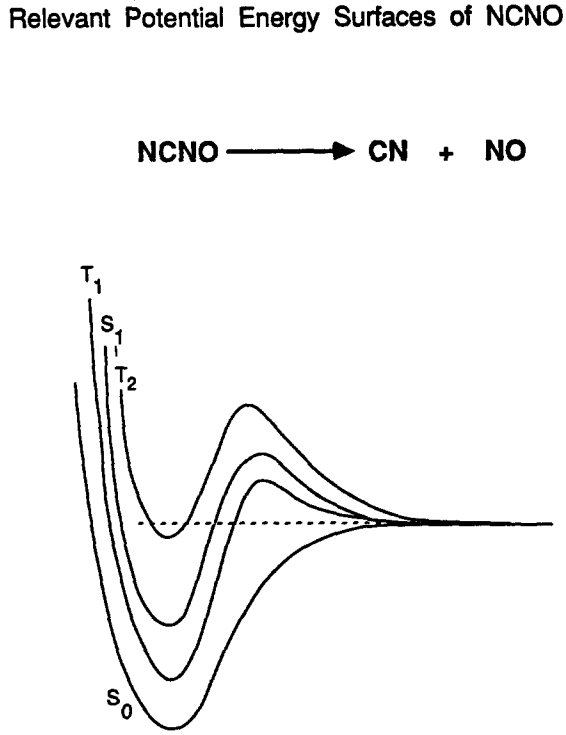

FIG. 1. Schematic potential energy diagram for the dissociation of NCNO into NC and NO, indicating singlet and triplet states.

Before proceeding with the determination of k_{EJ}'s using Eq. (1) several points are considered first: The fragments NC and NO each have a doubly degenerate ground state (spin degeneracy). In addition, NO has a doubly degenerate excited electronic state at 120 cm^{-1} excess energy, this splitting arising from a spin–orbit interaction ($j_{el} = 1/2,3/2$). In Fig. 1 a schematic correlation diagram is given for the present NCNO photodissociation. The initial photoexcitation involves excitation to the S_1 state. The latter state is calculated[9] to have a barrier height above the value at $R = \infty$ of 6674 cm^{-1}, and thus for excess energies below this amount either internal conversion to the S_0 (cf. Fig. 1) or intersystem crossing to the T_1 state must occur before dissociation can take place. Because of the usual rapidity of internal conversion processes the former occurs to S_0 before the dissociation, consistent with a number of observations (see Refs. 1 and 4). In the region of the TS there may be competitive "intersystem crossings" and "internal conversions" between the various states. However, the calculated barrier of 6674 cm^{-1} for the S_1 state indicates that the S_1 and T_2 states probably have little influence on the rates. In principle, they could play a role in a determination of the product state distributions in the case of PST, since in PST itself no detailed dynamics are postulated to restrict such usage of these states, and the states may be nearly degenerate at the large $R^{\dagger}(l)$'s involved in PST.

A general discussion of the role of the triplet level in RRKM calculations has been given in Ref. 8. The discussion there indicates that one approach to the rate calculations, in the case where the intersystem crossing rates and triplet po-

tential energy surfaces are not well known, and where there is some barrier in the triplet level, is to consider only the singlet state S_0. An alternative model is to consider a limiting case where the intersystem crossing rates in the TS region are very rapid and calculate an $N^{\dagger}_{EJ}(R)$ as the sum of the number of states for both the S_0 and T_1 states ($N_{EJ} = N^{S_0}_{EJ} + N^{T_1}_{EJ}$), each of which contains a degeneracy factor g_e which is one for the singlet state and three for the triplet state and each of which has its own potential energy function. Then the $R^{\dagger}$ at which this $N_{EJ}(R)$ has a minimum is calculated.

In order to perform the above calculation a potential energy surface for the triplet state T_1 is needed. This triplet state for NC + NO recombination is expected to be initially repulsive with a small barrier, before becoming attractive by an amount of about 11 000 cm^{-1} at is equilibrium configuration. (The singlet–triplet splitting is then about 6000 cm^{-1} or about half the singlet–singlet energy difference as in other nitroso compounds.[4]) Recent *ab initio* calculations[9] of the T_1 potential surface indicate that the barrier height above the value at infinite separation is 4600 cm^{-1}. This reasonably large barrier height suggests that the T_1 triplet state is not likely to play a major role in the determination of the dissociation rates.

Another point discussed elsewhere[8] is that in the expression for k_{EJ} given in Eq. (1) it is assumed that there is one dominant minimum in the number of states N_{EJ} as a function of the dissociation coordinate R. For highly flexible transition states there may, in fact, be two local minima in the plot of N_{EJ} vs R. In Sec. IV, results are given which indicate that although there are two local minima in the $N_{EJ}(R)$ plot for a certain energy range, the rate is still well described in the present case by merely using the principal minimum in $N_{EJ}(R)$ for $N^{\dagger}_{EJ}$.

One final consideration involves the determination of the density of states for the reactant molecule. For the present NCNO dissociation reaction the number of vibrational modes for the reactant is small enough that a direct count of the number of states is easily performed. Diagonal anharmonicities were included in the direct count used here. These diagonal anharmonicities were estimated through consideration of the frequencies and dissociation energies of the respective bonds. Their inclusion increased the density of states by a factor of only 1.25 at energies near the dissociation threshold of 17 085 cm^{-1}. Off-diagonal anharmonicities are expected to modify the density of states further, perhaps by a factor of similar magnitude. These off-diagonal anharmonicities were not included in the present density of states calculation, their values not being known. However, the correction due to these anharmonicities should be reasonably constant over the experimentally considered energy range of only 700 cm^{-1} for the rates.

III. REACTION RATE CONSTANT RESULTS

In this section the results of the present k_{EJ} calculations are compared with the experimental results of Ref. 1. Unless otherwise specified, the results given here are for the case of reaction on only the singlet state S_0. Also, all reaction rate calculations were performed for a total angular momentum quantum number J of 3, which is the estimate of its average value given in Refs. 1 and 4. The Monte Carlo error bars for the calculations presented here are in all cases less than 10%.

Before presenting these results, we first consider properties of the conserved and the transitional modes used here. In the absence of a detailed potential energy surface the conserved modes were treated as harmonic oscillators with an exponential interpolation between the reactant and product frequencies and reactant and product bond distances being used:

$$\lambda_i(R) = \lambda_i^p + (\lambda_i^r - \lambda_i^p)g(R), \tag{2}$$

where $g(R) = \exp[-\alpha(R - R_e)]$,[6,10] R_e is the equilibrium value of R for the reactants, and λ denotes ν or r_e, i denotes NC or NO, ν_{NC} and $r_{e,NC}$ are the terminal NC stretch frequency and separation distance, and ν_{NO} and $r_{e,NO}$ denote those of NO. The r and p superscripts denote the reactant (NCNO) and products (NC + NO), respectively. A value of 1.0 $Å^{-1}$ for the parameter α, which has been commonly found to provide agreement with experiment in the adiabatic channel model,[10] was used. The properties for the conserved modes are given in Table I, together with the frequencies and anharmonicities for the transitional modes of the reactant.

In the model of the potential energy surface assumed here for the transitional modes, the sum of a bonding potential for the central NC–NO bond and a nonbonding potential for the other interfragment interactions was used. The nonbonding potential was chosen to be a sum of 6-12 Lennard-Jones potentials for the van der Waals interactions between the nonbonded atoms of the two separate fragments, as in Eq. (3) below.[11] The bonding potential was approximated by a Varshni potential,[12,13] multiplied by an orientation factor which accounts for the loss of bonding which occurs when the fragments are improperly oriented. This factor was

TABLE I. Spectroscopic parameters for NCNO.

Parameter		Reactants value[a]	Products value[a]
(i) Frequencies (cm^{-1})	NC stretch	2170	2068.7
	NO stretch	1501	1904.03
	CN stretch	820	
	CNO bend	216.5	
	NCNbend	588.5	
(ii) Anharmonicities[b] (cm^{-1})	NC stretch	13.1	13.1
	NO stretch	14.1	14.1
	CN stretch	9.4	
	CNO bend	0.2	
	NCN bend	0.5	
Coordinates	R_e	2.4 Å	
	$r_{e,NC}$	1.163 Å	1.1718 Å
	$r_{e,NO}$	1.217 Å	1.1508 Å
	$\theta_{e,CNO}$[c]	120°	
	$\theta_{e,NCN}$[c]	180°	

[a] Unless stated otherwise, all values are as specified in Ref. 4.
[b] Anharmonicities have been obtained from Ref. 4 or estimated from the dissociation energy.
[c] The values used correspond to sp and sp^2 bonding geometries rather than to the equilibrium bending angles.

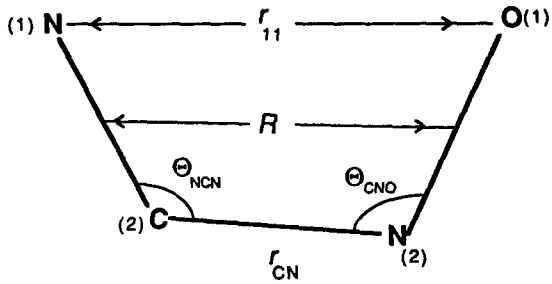

FIG. 2. Coordinates used in describing the potential energy of the transitional modes of NCNO.

chosen to be $\cos^2(\theta_{NCN} - \theta_{e,NCN})\cos^2(\theta_{CNO} - \theta_{e,CNO})$ when both $|\theta_{NCN} - \theta_{e,NCN}|$ and $|\theta_{NCN} - \theta_{e,NCN}|$ are less than $\pi/2$. Otherwise the factor is set equal to zero. (No bonding is assumed to occur when the angles are outside that range.) Here, θ_{NCN} and θ_{CNO} are the NCN and CNO bending angles, respectively, while $\theta_{e,NCN}$ and $\theta_{e,CNO}$ denote their equilibrium values, as given in Table I. These coordinates are illustrated in Fig. 2 along with the other coordinates used in describing the potential energy for the NCNO transitional modes. The Varshni potential rather than a Morse potential was employed since the latter is known[10,13] to decay to zero too slowly at large separation distances, whereas the former is believed to provide a better representation for this region.[13]

Assuming this representation of the nonbonding potential V_{LJ} in terms of van der Waals interactions we have

$$V_{LJ} = \sum_{i,j=1}^{2}{}' 4\epsilon_{ij}[(\sigma_{ij}/r_{ij})^{12} - (\sigma_{ij}/r_{ij})^{6}], \tag{3}$$

where i and j label atoms in the NC and NO fragments, respectively, and the prime indicates that the central NC–NO bond is not included in the sum. The parameters σ_{ij} and ϵ_{ij} denote the usual Lennard-Jones parameters for the interaction between atoms i and j; r_{ij} is then the separation distance between atoms i and j. The Varshni potential V_V for the NC–NO bond, denoted by CN in Eq. (4), is given by the standard form[12,13]

$$V_V = D_{CN}\left\{1 - \left(\frac{r_{e,CN}}{r_{CN}}\right)\exp[-\beta_{CN}(r_{CN}^2 - r_{e,CN}^2)]\right\}^2 - D_{CN}. \tag{4}$$

The parameters for this model potential energy surface for the transitional modes are given in Tables II and III. The parameters for the Lennard-Jones potential V_{LJ} (Table II) were taken for convenience to be the same as those which

TABLE II. Lennard-Jones potential parameters for NCNO.

Parameter	Value[a]	Parameter	Value[a]
σ_{CO}	3.36 Å	ϵ_{CO}	51.9 cm^{-1}
σ_{NN}	3.25 Å	ϵ_{NN}	59.5 cm^{-1}
σ_{NO}	3.11 Å	ϵ_{NO}	46.7 cm^{-1}

[a] All values have been obtained from Ref. 14 making use of the combination rules $\epsilon_{ij} = (\epsilon_{ii}\epsilon_{jj})^{1/2}$ and $\sigma_{ij} = \frac{1}{2}(\sigma_{ii} + \sigma_{jj})$.

TABLE III. Varshni potential parameters for NCNO.

Surface	Parameter	Assumed potential[a]	Effective potential
I	$r_{e,CN}$	1.418 Å	1.2 Å
	β_{CN}	0.48 $Å^{-2}$	0.517 $Å^{-2}$
	D_{CN}	17 880 cm^{-1}	32 110 cm^{-1}
II	$r_{e,CN}$	1.418 Å	1.2 Å
	β_{CN}	0.70 $Å^{-2}$	0.7725 $Å^{-2}$
	D_{CN}	17 880 cm^{-1}	42 600 cm^{-1}

[a] The parameter β_{CN} was obtained by setting $\partial^2 V_{varsh}/\partial r_{CN}^2 = k$, where k is the force constant for the central CN stretch given in Ref. 15. For surface II β_{CN} was arbitrarily set to 0.70 $Å^{-2}$. All other parameters of the assumed potential are as determined spectroscopically in Ref. 4.

gave good results in Monte Carlo simulations of amides and peptides.[14] The parameters D_{CN} and β_{CN} of the Varshni potential were chosen to fit the *total* potential energy function to an assumed Varshni potential surface for the NC–NO separation distance in the range of 3.3 Å. The parameters for this assumed Varshni potential surface are given in Table III and were determined here from a consideration of the spectroscopic constants and the force constants determined by Wilson G-matrix analysis of the harmonic frequencies in Ref. 15. The parameter $r_{e,CN}$ for the fitted potential was held fixed at 1.2 Å. The results depended relatively little on this parameter.

Results for k_{EJ} calculations for the above model of the potential energy surface are given in Fig. 3, where the dissociation rates are plotted vs energy. Also given for comparison in Fig. 3 are results for the case in which T_1 is included (but with no barrier–the dashed line in Fig. 1) and in which the intersystem crossing rate in the TS region is assumed to be much larger than the dissociation rates. Recent *ab initio*

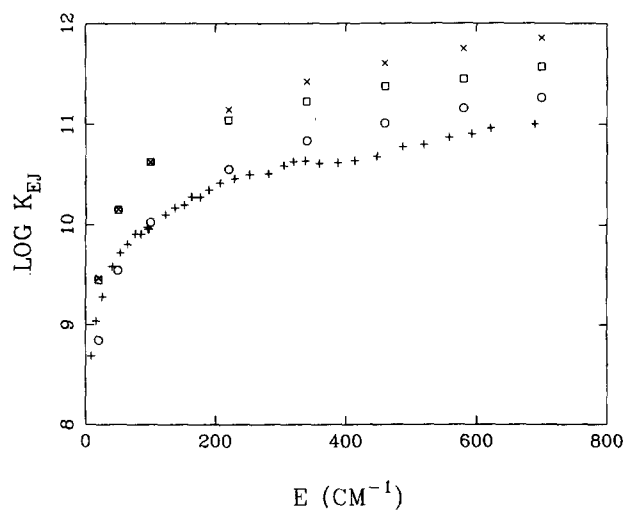

FIG. 3. Plot of theoretically determined rate constants log k_{EJ} vs energy for a variety of treatments of the T_1 triplet surface, and plot of the experimentally determined rate constants (plus signs). The circles denote RRKM calculations on the singlet surface only, boxes denote RRKM calculations including the singlet and a flat triplet surface with a degeneracy of three for the triplet. The ×'s are given for comparison and denote a PST calculation which includes both the S_0 and T_1 states.

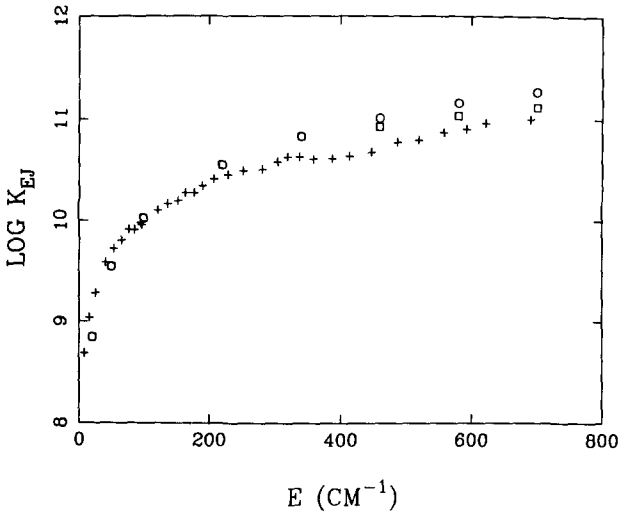

FIG. 4. Plot of theoretically determined rate constants log k_{EJ} vs energy for two different assumed parameters for the Varshni bonding potential, and a plot of the experimentally determined rate constants (plus signs). The circles denote RRKM calculations for an assumed potential with a β parameter of 0.48 $Å^{-2}$, boxes denote RRKM calculations for an assumed potential with a β parameter of 0.70 $Å^{-2}$. Both are for the singlet-only calculation. Below 400 cm^{-1}, the results for the circles and boxes are essentially identical.

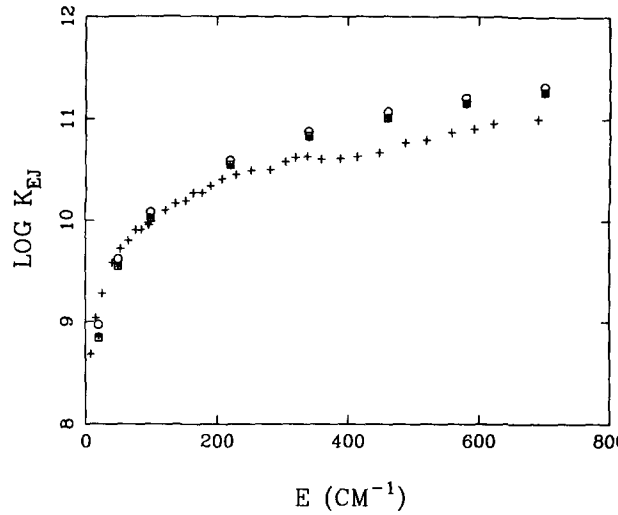

FIG. 5. Plot of rate constants log k_{EJ} vs energy as determined via quantum PST, classical PST and $N_{EJ}(\infty)$ and a plot of the experimentally determined rate constants (plus signs). Circles denote quantum PST calculations, asterisks the classical PST calculations, and boxes the $N_{EJ}(\infty)$ calculation, all for the singlet-only calculation.

calculations show, however, as noted earlier, that the triplet state T_1 is even more repulsive than this simplified model. The result of this is that the contribution from T_1 state will be considerably less than that shown in Fig. 3 and that it will also disappear at lower excess energies. This contribution will also be considerably smaller if the rates of crossing between the S_0 and the T_1 states are not large in the TS region. For comparison the results of a PST calculation which includes both S_0 and T_1 states are also given in Fig. 3. In PST one typically considers the degeneracies at $R = \infty$ [because the $R^{\dagger}(l)$'s of PST are usually quite large] in which case the T_1 state contributes an extra factor of 3.

Results are given in Fig. 4 for a potential energy surface for which the dissociative singlet state (S_0) potential has been fit to an assumed β parameter of 0.7 $Å^{-2}$ rather than 0.48 $Å^{-2}$. The resulting parameters for this surface are also given in Table III and labeled as potential surface II, the $\beta = 0.48$ $Å^{-2}$ surface being labeled I.

Results of three types of PST calculations are given in Fig. 5. They involve a classical PST integral over phase space, a quantum PST sum over quantum states, and a calculation in which $N_{EJ}(\infty)$ is used for $N^{\dagger}_{EJ}$ in Eq. (1). (The latter calculation corresponds to a PST calculation in which the l-dependent barriers are all at "infinite" separation. While the l-dependent barriers in PST can never be at infinity, they can be at such a large separation distance that the effective barrier energy, a centrifugal potential plus an attractive potential, is negligible.) The PST calculations have all been performed as described in Refs. 1 and 4 with a C_6 potential parameter of 1.6×10^5 cm^{-1} $Å^6$, the only difference being that in the present PST rate calculations only the S_0 state is considered.

IV. REACTION RATE DISCUSSION

The results given in Fig. 3 indicate that the contribution of the "flat PES" triplet to the rate varies from three times that of the singlet state at energies near the threshold for dissociation to comparable with that of the singlet state at an excess energy of 700 cm^{-1}. This disappearing contribution of the triplet state occurs as the rate changes from being determined mainly by the number of states at $R = \infty$ to being determined mainly by the number of states at the inner minimum in N_{EJ}. This effect reflects the R of the inner minimum in the number of states being small enough that the singlet–triplet gap for the present model surfaces is comparable to or larger than the excess energy. That is, when this inner minimum in N_{EJ} is less than about 4 Å the difference between the minimum potential energy for a given R on the singlet and flat triplet states becomes quite large, while at the same time the orbital kinetic energy of the two fragments is becoming relatively large, resulting in a much lower number of states for the triplet potential surface. In PST the typical R values for the purely l-dependent barriers of PST do not become this small until much higher energies are reached and so the contribution from the triplet remains considerable until much higher energies. The above described effect on the number of states is illustrated schematically in Fig. 6. As noted earlier, if the barrier on the T_1 surface is included, rather than just using a flat surface, the T_1 contribution would be considerably less than that indicated in Fig. 3.

The results given for the excess energies E of at most 700 cm^{-1} in Fig. 3 for dissociation on the singlet state only are quite similar to the PST results for the singlet state shown in Fig. 5. This similarity arises because at these energies the "inner minimum" in the number of singlet states N_{EJ} is about the same or more than the number of singlet PST states (the T_1 triplet state is being neglected). At higher energies this value of this minimum of N_{EJ} actually becomes

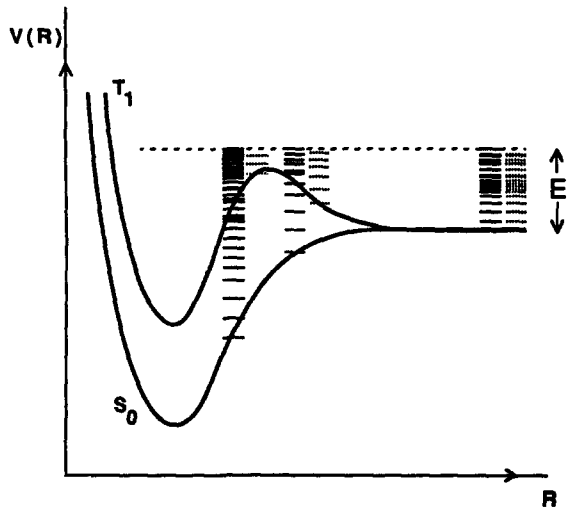

FIG. 6. Schematic plot of the change in the number of states with separation distance R for both the S_0 and T_1 states. The dashed line denotes a given energy E. The solid and dashed bars denote the states of energy less than E on the singlet and triplet surfaces, respectively.

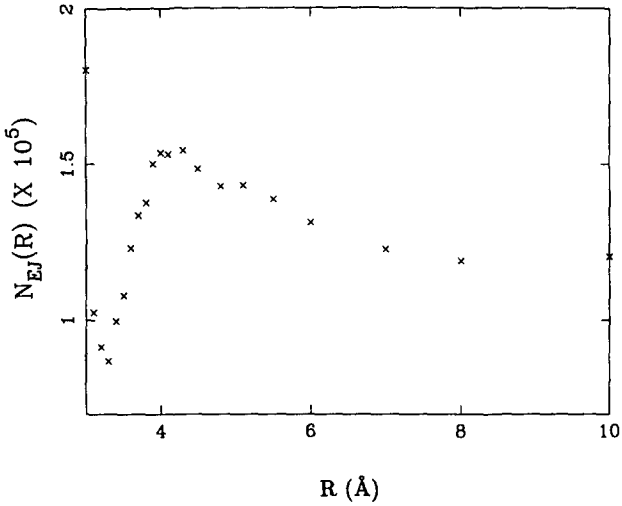

FIG. 8. As in Fig. 7 but for an excess energy of 700 cm^{-1}.

less than that for PST and so, within the framework of the present potential energy surface, this new minimum represents a better transition state. This effect can be seen in Figs. 7–9, where plots of $N_{EJ}(R)$ vs R are given for the $\beta = 0.7$ $Å^{-2}$ potential energy surface at the three energies, 50, 700, and 2000 cm^{-1}. The results in Figs. 7–9 indicate that with increasing energy the inner minimum becomes more and more the dominant minimum.

There are two parts of the potential energy surface function which can significantly affect the calculated rates: the dissociative and the hindered rotational potentials. If the central C–N dissociative potential actually approaches zero more rapidly than that given by the Varshni potential energy surface considered in Fig. 3 the results start to deviate from PST results at lower energies. This effect can be seen in Fig. 4, where results are given for the different values of the β parameter. In this case for a $\beta = 0.70$ $Å^{-2}$ the RRKM results already differ from those of PST by a factor of 0.71 at an $E = 700$ cm^{-1}. The calculated rates also depend on the strength and location of the attractive wells of the Lennard-Jones potentials describing the hindered rotation of the fragments. While results for this case are not presented here, when one increases σ_{ij} by about 0.3 Å, the results are analogous to those obtained for the larger β parameter study. That is, moving the van der Waal's repulsion outward has a similar effect to moving the bonding potential to smaller R's.

The results in Fig. 5 indicate that classical PST and the $N_{EJ}(\infty)$ treatments of the transitional modes are very similar for these energies, with the differences being only about 1% to 2%. This similarity occurs because for the energies employed in the experimental work in Ref. 1 the assumed attractive potential in PST is essentially such a long range potential that $R^{\dagger}(l)$ is so large that the effective barrier is negligible for even the largest l's present. If these l-dependent barriers were completely negligible then the $N_{EJ}(\infty)$ and

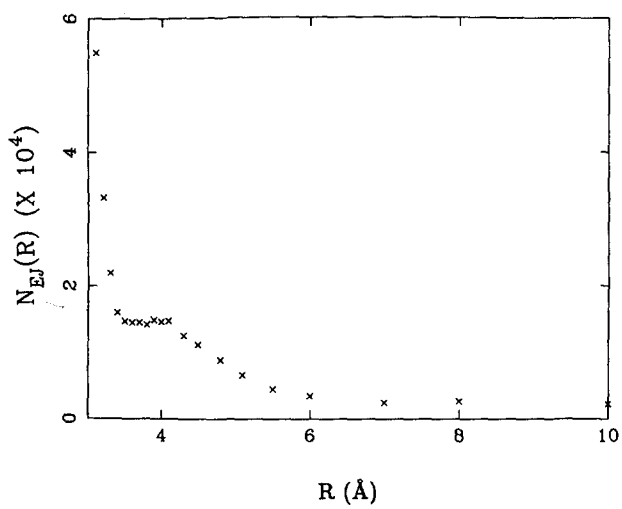

FIG. 7. Plot of number of states $N_{EJ}(R)$ vs separation distance R for potential energy surface II for an excess energy of 50 cm^{-1}.

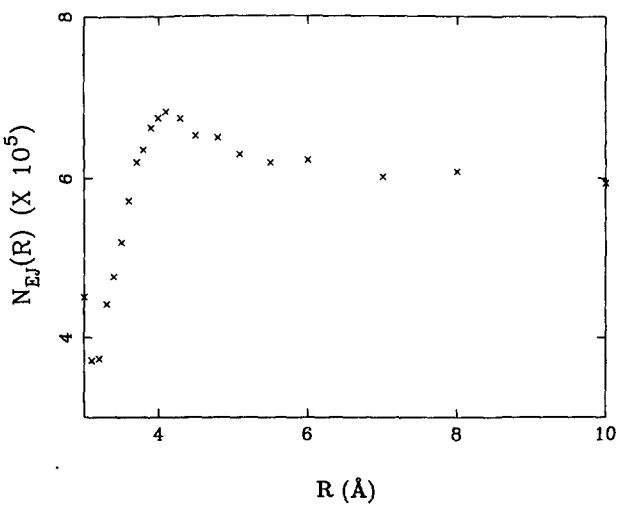

FIG. 9. As in Fig. 7 but for an excess energy of 2000 cm^{-1}.

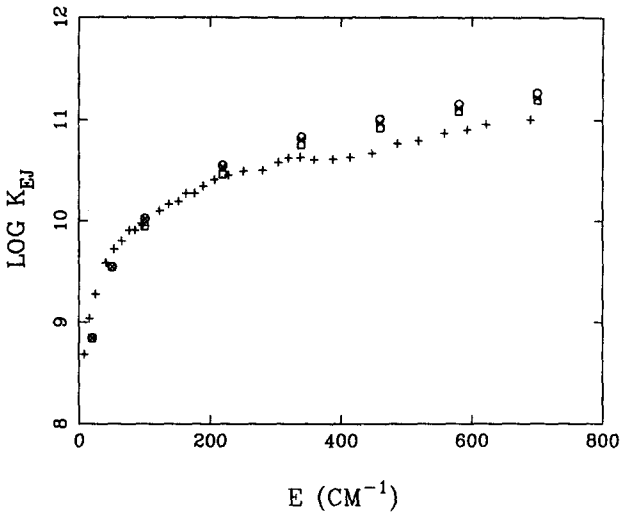

FIG. 10. Plot of rate constants log k_{EJ} vs energy when the two minima in $N_{EJ}(R)$ plot are taken into account, and a plot of the experimentally determined rate constants (plus signs). The ×'s denote the use of the unified statistical theory of Ref. 16, boxes refer to the use of the lower bound of Ref. 17, and circles refer to the use of the overall minimum. All are for the singlet-only calculation.

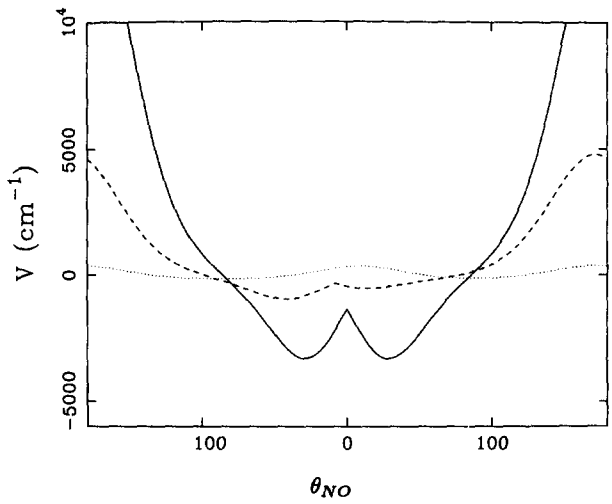

FIG. 12. As in Fig. 11 with the dependence of potential energy surface I on θ_{NO} for $R = 3.5$ Å, and $\phi_{NC} = 0$. Plots for $\theta_{NC} = 0°$, 45°, and 90° are given by the solid, dashed, and dotted lines, respectively. The left half of the plot corresponds to $\phi_{NO} = 180°$, while the right half corresponds to $\phi_{NO} = 0°$.

classical PST calculations would give identical results. Similarly, the classical and quantum phase space theory results are in good agreement, with the classical calculation being typically 10% to 15% below the quantum one. Finally, it is also interesting to note that when only the singlet surface S_0 is considered, the present results using the different types of PST or using RRKM theory are in better agreement with the experimental results than the PST calculations given in Fig. 14 of Ref. 1, where the electronic degeneracy was treated simply as some constant over the energy range with a second contribution arising from the upper singlet and triplet states whose asymptotic energy is 120 cm^{-1} above that of the lower singlet and triplet.

In Fig. 10 the results from three methods for taking into account the presence of two minima in the $N_{EJ}(R)$ plot are given. The simplest method is to take $N^{\dagger}_{EJ}$ as the overall minimum in $N_{EJ}(R)$ and this is what has been done in Figs. 3 and 4 here. In another method, termed unified statistical theory,[16] statistical reflection and transmission probabilities are introduced to obtain $N^{\dagger}_{EJ}$. In a third method[17] a lower bound is determined (within certain dynamical assumptions) to $N^{\dagger}_{EJ}$. Formulas for these different treatments are summarized in Ref. 8. The results plotted in Fig. 10 for potential surface I indicate that in the present case the effect of

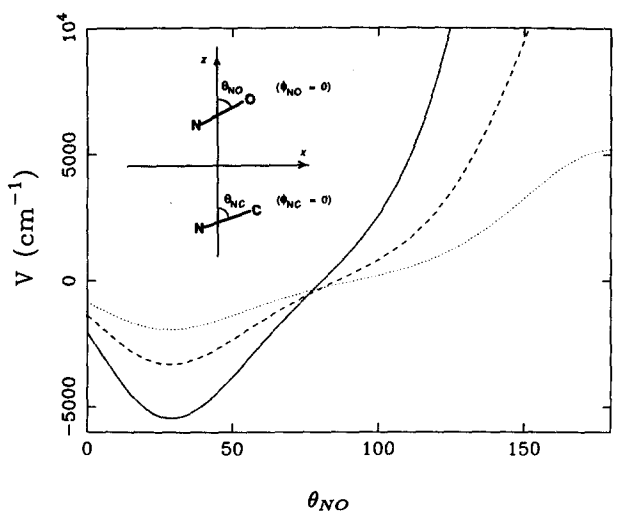

FIG. 11. Plot of potential energy surface I, as a function of θ_{NO} for a variety of R's in the transition state region. θ_{NO} and ϕ_{NO} are the polar angles which describe the orientation of the NO fragments. Similarly, θ_{NC} and ϕ_{NC} are the polar angles describing the orientation of the NC fragment (e.g., see inset). The equilibrium orientation is for $\theta_{NO} \approx 30°$ and $\theta_{NC} \approx 0°$. The dependence of the potential energy on θ_{NO} for $\theta_{NC} = 0°$, $\phi_{NO} = 0°$, and $\phi_{NC} = 0°$. Plots for $R = 3.3$, 3.5, and 3.7 Å are given by the solid, dashed, and dotted lines, respectively.

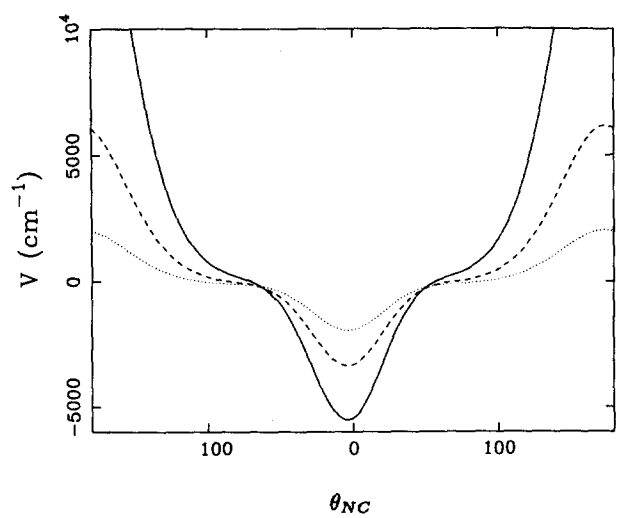

FIG. 13. The dependence of potential energy surface I on θ_{NC} for $\theta_{NO} = 30°$ and $\phi_{NO} = 0°$. Plots for $R = 3.3$, 3.5, and 3.7 Å are given by the solid, dashed, and dotted lines, respectively. The left half of the plot corresponds to $\phi_{NC} = 180°$, while the right half corresponds to $\phi_{NC} = 0°$.

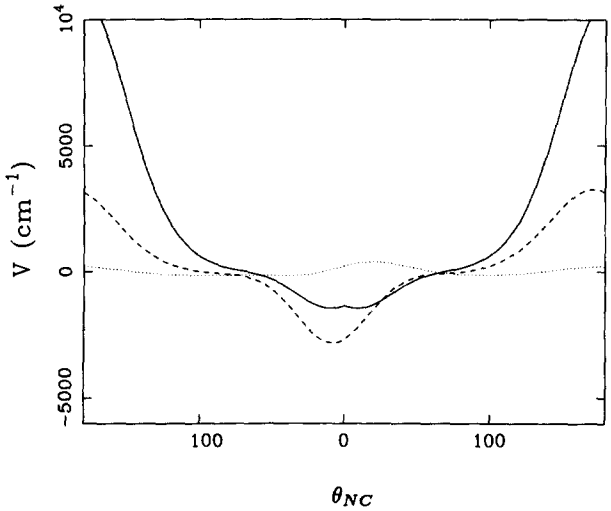

FIG. 14. The dependence of potential energy surface I on θ_{NC} for $R = 3.5$ Å and $\phi_{NO} = 0°$. Plots for $\theta_{NO} = 0°$, 45°, and 90° are given by the solid, dashed, and dotted lines, respectively. The left half of the plot corresponds to $\phi_{NC} = 180°$, while the right half corresponds to $\phi_{NC} = 0°$.

there being two minima was at most a factor of 0.8. Similar results for potential surface II indicate that the effect was at most a factor of 0.5.

In Figs. 11–14 the dependence of the present potential energy surfaces on certain bending angles are presented for typical $R^\dagger$'s. These figures are given for a range of R where an *ab initio* determination of the potential surface for the transitional modes would be especially useful for obtaining improved bending and hindered rotational potential energy surfaces. In particular, from these figures it is seen that in the TS region the absolute minimum in the potential for a given R is negative and has a magnitude of a few thousand cm^{-1} while the rotational barriers are positive and have a much larger magnitude.

V. PRODUCT STATE DISTRIBUTIONS

In order to calculate vibrational and rotational distributions of the products using RRKM theory some dynamical assumption needs to be introduced regarding the motion in the exit channel. In particular, it was assumed in Ref. 5 that the conserved modes are adiabatic from $R^\dagger$ to $R = \infty$, and that the transitional modes, which are usually of low frequency in the TS region, behave quite differently. Namely, it was assumed that these transitional modes may freely interchange energy from $R^\dagger$ to $R^\dagger(l)$, the position of the loose (PST) transition state. In implementing such a theory, the number of states $N_{EJi}(R)$ for a state of excitation i of the conserved modes is calculated and its minimum found, at $R = R_i^\dagger$, say, as in Eq. (6) of Ref. 5. [The corresponding rate expression is given by Eq. (7) there.] This procedure is followed in obtaining the results in Table IV. A more approximate procedure is to remove from $N_{EJ}(R^\dagger)$ any states i whose channels are "closed" at $R = \infty$, as discussed in Ref. 5. We have used this procedure also. It entails less calculation, particularly at large E's, since only one $R^\dagger$ is required instead of an $R_i^\dagger$ for each i.

In each case, using this vibrational distribution the rotational distribution is then calculated from the statistics at $R^\dagger(l)$.[5] It is important to note that even after passing through the TS which determines the rate constant the fragments may continue to interact and cross from one electronics state to another. It is therefore assumed that the degeneracies of the product states may be used in determining the rotational and electronic state distributions. This assumption is based in part on the observation that the PST $R^\dagger(l)$ are at large separation distances. This assumption differs from the assumption used in the rate constant calculations where the $R^\dagger$'s determined from the variational-RRKM theory calculations indicated that for the rate determinations only the S_0 state should be used. In effect, this use of only the S_0 state in the rate calculations is based on our knowledge from the variational-RRKM calculations that the other states do not contribute to the rate even though the $R^\dagger(l)$'s of PST indicate that they could.

For energies below the threshold for vibrational excitation of the products the product state distributions predicted by the theory described in Ref. 5 are identical to the PST determined distributions. Also, the present detemination of the PST distributions is identical to that of Ref. 4 since the product state degeneracies are used in both cases. These product state distributions have been described in detail in Ref. 4 and so will not be repeated here. For energies above the vibrational excitation threshold calculations have been performed as described in Secs. III and IV except that the conserved modes were treated as Morse rather than harmonic oscillators and now the total angular momentum quantum number J was taken to be 5 so as to compare with the previous experiments of Nadler *et al.*[4] Potential surface I was used.

Plots of the NO and NC rotational distributions, determined by the above method are given in Figs. 15–17. Also given there are the corresponding plots determined experimentally and by PST. The results of Fig. 15 indicate that the theory of Ref. 5 provides an improvement over PST in describing the CN rotational state distributions at excitation energies above the vibrational threshold. For the case of the NO rotational distributions given in Figs. 16 and 17 the ex-

TABLE IV. Vibrational distributions for NCNO at different excess energies.

Vibrational level	Excess energy (cm^{-1})	Vibrational distributions			
		Expt.	$R_i^\dagger$[a]	$R^\dagger$[b]	PST
$v_{CN} = 1$	2348	0.07 ± 0.02	0.07	0.08	0.034
$v_{NO} = 1$	2348	0.12 ± 0.03	0.13	0.16	0.07
$v_{CN} = 1$	2875	0.16 ± 0.02	c	0.14	0.11
$v_{CN} = 1$	3514	0.20 ± 0.03	c	0.17	0.17
$v_{CN} = 1$	4050	0.24 ± 0.03	c	0.23	0.20
$v_{CN} = 1$	4269	0.27 ± 0.04	c	0.22	0.21

[a] $R_i^\dagger$ corresponds to the use of the minimum of $N_{EJi}(R)$ for each vibrational level i.

[b] $R^\dagger$ corresponds to the use of the minimum of $N_{EJ}(R)$. The values of $R^\dagger$ for $E = 2348$, 2348, 2875, 3514, 4050, and 4269 cm^{-1} are 3.3, 3.3, 3.1, 3.0, 3.0, 3.0 Å, respectively.

[c] Not all $R_i^\dagger$'s are known.

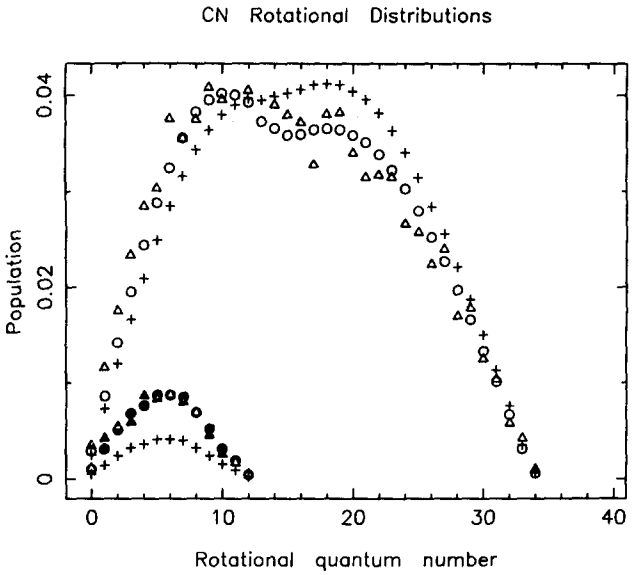

FIG. 15. Plot of CN rotational distribution for both the $v = 0$ and the $v = 1$ CN vibrational states at an excess energy of 2348 cm^{-1}. For $v = 0$ the triangles denote the experimental results, the circles the present RRKM results, and the pluses the PST results. For $v = 1$ the boxes denote the experimental results, the $\times$'s the present RRKM results, and the asterisks the PST results.

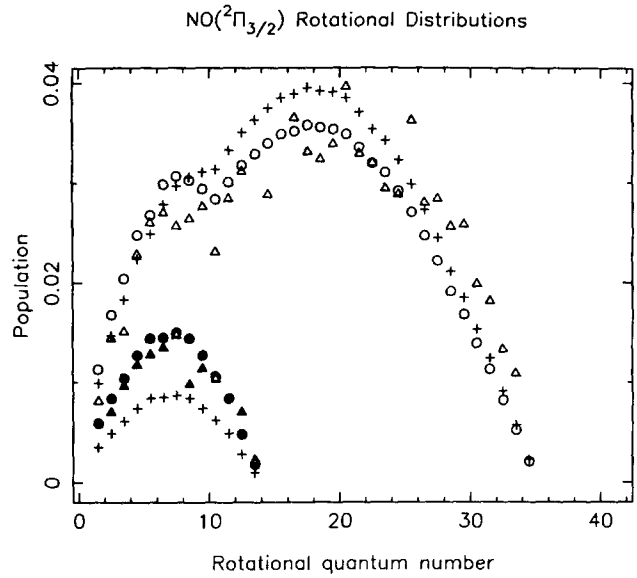

FIG. 17. As in Fig. 16 but for the NO($^2\Pi_{3/2}$) state.

perimental scatter obscures the comparison between the different theories.

In Table IV the vibrational distributions calculated from the present implementation of RRKM theory are compared with those determined both experimentally and from PST by Nadler *et al.*[4] It is seen from Table IV that the RRKM distributions for the excess energies of 2348 and 2875 cm^{-1} are in better agreement with the experimental distributions than are the PST distributions. The RRKM theory distributions based on the use of an $R_i^\dagger$ for each vibrational state i could not be determined for excess energies higher than 2500 cm^{-1} because the assumed Lennard-Jones potentials were so strongly repulsive in this region that for some vibrational states there was no local minimum in the $N_{EJi}(R)$ plot. Indeed, by calculating $N_{EJ}(R)$ at the equilibrium value of R in the NCNO molecule, where $N_{EJ}(R)$ is known, it is clear that the Lennard-Jones/Varshni combination does not yield at $R = R_e$ a good result for $N_{EJ}(R)$, since R is so small. There is no reason why it should. Instead, Lennard-Jones potentials might only be accurate at low excess energies, corresponding to quite large $R^\dagger$'s. Thus, the need for accurate *ab initio* potentials for the transitional modes is once again emphasized.

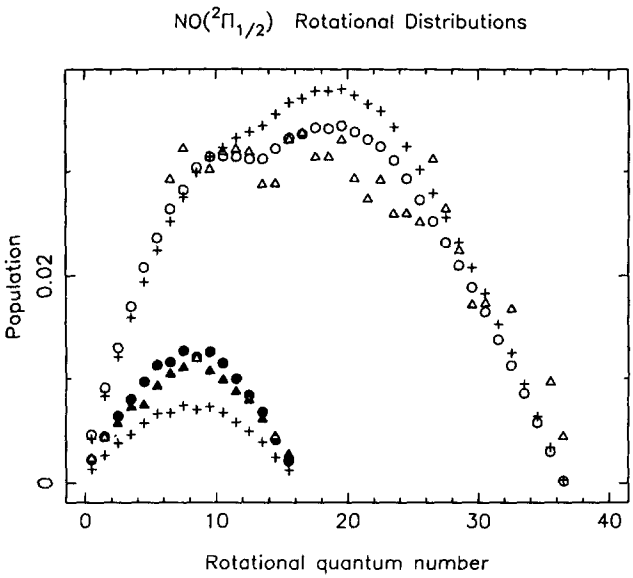

FIG. 16. Plot of NO($^2\Pi_{1/2}$) rotational distribution for both the $v = 0$ and $v = 1$ NO vibrational states at an excess energy of 2348 cm^{-1}. The triangles denote the experimental results, the circles the present results, and the pulses the PST results. The $v = 1$ results are the ones with the lower populations.

Nadler *et al.* have obtained similar improved agreement with the experimental vibrational–rotational distributions at excess energies above the vibrational threshold.[4] In their modification of PST, labeled SSE, they calculated, in effect, the vibrational distribution for a constant l in the exit channel and neglected the centrifugal and radial potentials. The resulting vibrational distribution was then used to determine the full rotational–vibrational distribution from PST.

VI. CONCLUDING REMARKS

An implementation of RRKM theory for highly flexible transition states has been applied to the NCNO dissociation reaction. The ground singlet state S_0 is most likely the only state contributing significantly to the rate constants. The results also indicate that the rate constants determined from the present *variational*-RRKM theory are similar to the PST results for the S_0 state only with some differences at the highest energies studied. Both of these theories also provide agreement (Fig. 5) with the experimental results, with only apparent plateau regions not being explained. The results for the rotational–vibrational distributions indicate that the

RRKM theory based on the method of Ref. 5 may explain the difference between the experimental and the PST rotational–vibrational distributions at energies above the vibrational excitation threshold. One common aspect of the results presented here is the dependence on the values used for the potential surface parameters. Also, not all of $R_i^{\dagger}$'s for use in the determination of the product state distributions could be determined for excess energies above about 2500 cm^{-1} due to the inaccuracy of a repulsive Lennard-Jones-type surface at these high energies. Thus, an accurate *ab initio* potential energy surface for the TS region is highly desirable.

Similar calculations are now underway to relate the experiments of the Moore (product state distribution) and Zewail (state to state rates) groups on the photodissociation of CH_2CO into CH_2 and CO.

ACKNOWLEDGMENTS

It is a pleasure to acknowledge the support of this research by the National Science Foundation. We are indebted to Professor G. Segal for providing us with results of his calculated potential energy surfaces and to Professor H. Reisler for supplying the experimental data used in Figs. 16 and 17.

[1]L. R. Khundkar, J. L. Knee, and A. H. Zewail, J. Chem. Phys. **87**, 77 (1987).

[2]P. J. Robinson and K. A. Holbrook, *Unimolecular Reactions* (Wiley, New York, 1972); W. Forst, *Theory of Unimolecular Reactions* (Academic, New York, 1973); R. E. Weston and H. A. Schwarz, *Chemical Kinetics* (Prentice–Hall, Englewood Cliffs, NJ, 1972); R. A. Marcus, J. Chem. Phys. **20**, 359 (1952); R. A. Marcus and O. K. Rice, J. Phys. Colloid. Chem. **55**, 894 (1951); R. A. Marcus, J. Chem. Phys. **43**, 2658 (1965); **52**, 1018 (1970).

[3]P. Pechukas and J. C. Light, J. Chem. Phys. **42**, 3281 (1965); P. Pechukas, R. Rankin, and J. C. Light, *ibid.* **44**, 794 (1966); C. Klotz, J. Phys. Chem. **75**, 1526 (1971); C. Klotz, Z. Naturforsch. Tiel A **27**, 553 (1972); W. Chesnavich and M. Bowers, J. Chem. Phys. **66**, 2306 (1977).

[4]I. Nadler, J. Pfab, G. Radhakrishnan, H. Reisler, and C. Wittig, J. Chem. Phys. **79**, 2088 (1983); I. Nadler, J. Pfab, H. Reisler, and C. Wittig, *ibid.* **81**, 653 (1984); M. Noble, I. Nadler, H. Reisler, and C. Wittig, *ibid.* **81**, 4333 (1984); I. Nadler, M. Noble, H. Reisler, and C. Wittig, *ibid.* **82**, 2608 (1985); C. Wittig, I. Nadler, H. Reisler, M. Noble, J. Catanzarite, and G. Radhakrishnan, *ibid.* **83**, 5581 (1985); C. X. W. Qian, M. Noble, I. Nadler, H. Reisler, and C. Wittig, *ibid.* **83**, 5573 (1985).

[5]R. A. Marcus, Chem. Phys. Lett. **144**, 208 (1988).

[6]D. M. Wardlaw and R. A. Marcus, Chem. Phys. Lett. **110**, 230 (1984); J. Chem. Phys. **83**, 3462 (1985); J. Phys. Chem. **90**, 5383 (1986); Adv. Chem. Phys. **70**, 231 (1988).

[7]S. J. Klippenstein and R. A. Marcus, J. Phys. Chem. **92**, 3105 (1988).

[8]S. J. Klippenstein and R. A. Marcus, J. Phys. Chem. (in press).

[9]Y. Y. Bai and G. A. Segal (to be published).

[10]M. Quack and J. Troe, Ber. Bunsenges. Phys. Chem. **78**, 240 (1974); J. Troe, J. Phys. Chem. **88**, 4375 (1984).

[11]The effect of the Coulombic potentials between the partial charges on the different atoms which are typically included in molecular dynamics simulations were also considered here. They were found to have a negligible effect on the number of states and so were neglected in the calculations presented here.

[12]Y. P. Varshni, Rev. Mod. Phys. **29**, 664 (1957).

[13]R. J. Duchovic, W. L. Hase, B. Schlegel, M. J. Frisch, and K. Raghavachari, Chem. Phys. Lett. **89**, 120 (1982); R. J. Duchovic and W. L. Hase, Chem. Phys. Lett. **110**, 474 (1984); D. Steele, E. R. Lippincott, and J. T. Vanderslice, Rev. Mod. Phys. **34**, 239 (1962).

[14]W. L. Jorgensen and C. J. Swenson, J. Am. Chem. Soc. **107**, 569 (1985).

[15]B. Bak, F. M. Nicolaisen, O. J. Nielsen, and S. Skaarup, J. Mol. Struct. **51**, 17 (1979).

[16]J. O. Hirschfelder and E. Wigner, J. Chem. Phys. **7**, 616 (1939); W. H. Miller, *ibid.* **65**, 2216 (1976); W. J. Chesnavich, L. Bass, T. Su, and M. T. Bowers, *ibid.* **74**, 2228 (1981); S. N. Rai and D. G. Truhlar, *ibid.* **79**, 6046 (1983).

[17]E. Pollak and P. Pechukas, J. Chem. Phys. **70**, 325 (1979); E. Pollak, M. S. Child, and P. Pechukas, *ibid.* **72**, 1669 (1980).